Automated photovoltaic module imaging for high throughput data capture and analysis

MT Sivewright [1], EE Van Dyk[2] and FJ Vorster[2]

Department of Physics, Nelson Mandela University, Port Elizabeth, South Africa

E-mail: s223099996@mandela.ac.za

Abstract. Photovoltaic (PV) module imaging has become a critical tool for assessing the performance, reliability, and degradation of PV modules. Automated imaging systems that use advanced hardware and image processing software tools allow for efficient high-throughput data capture across large-scale solar installations. These systems use different imaging techniques such as visible light (RGB) imaging, Thermal Infrared (TIR) imaging, ultraviolet fluorescence (UVF) imaging, electroluminescence (EL) imaging, and line sensor scanning. These imaging techniques allow for the detection of faults or anomalies in PV modules. We report on a project focusing on the development of a system for high-throughput visual and UV-F imaging of PV modules deployed in utility-scale PV plants. The work follows a two-step approach whereby two systems will be built. The first step consists of a laboratory-based imaging system to test the proof of concept. This system utilizes an Arduino MEGA 328P microcontroller for position control and a Raspberry Pi 5 8 GB microprocessor for sensor control, image capturing and storage. The images are then processed later through stitching and basic visual classification. The second step will use techniques determined to be effective from the initial system to build an onsite imaging and sensing system that allows for rapid, large-scale image capture for further image processing and classification. This allows for more data and images to be captured and thus processed as opposed to manual methods. At the same time, this method has a much greater resolution as opposed to drone imaging. This paper presents the design, manufacture, optimization and preliminary results from the laboratory-based system.

1 Introduction

Crystalline silicon (c-Si) PV modules consist of multiple bonded materials - glass, encapsulant, cells, interconnections, and backsheet - forming several interfaces. These interfaces can act as pathways for contaminants, causing degradation and reducing performance [1]. Effective encapsulation is essential for ensuring module reliability and extending operational life. Field inspections have shown that degradation related to poor encapsulation is a common cause of PV system failure. Proper encapsulation protects against moisture, UV radiation, and mechanical stress, helping the module retain stable performance over time [1].

A fault in a PV module occurs when its power output is lower than expected due to either temporary factors (e.g., shading, dirt) or permanent issues (e.g., cracks, encapsulant degradation, disconnections) [2]. Fault detection techniques help identify these issues and, although some may overlap, they enable comprehensive module characterization [2]. These techniques are typically categorized into DC and AC side methods, with the DC side further divided into electrical and imaging-based approaches [2]. The main imaging techniques are visual

inspection, thermal infrared (TIR), and electroluminescence (EL) [2], [3]. For effective detection, a technique should: (A) detect faults without disrupting power, (B) localize the fault, (C) be cost-effective and adaptable, (D) have a simple structure, and (E) apply to various PV systems [4].

Existing visual inspection methods often rely on manual image capture for each PV module [5]. While this approach provides high-resolution imagery and is suitable for small-scale systems, it becomes impractical and costly for large-scale PV plants due to the time and labour involved [5]. Unmanned Aerial Vehicles (UAVs) offer a faster alternative but are limited by lower image quality and susceptibility to weather conditions [5]. Moreover, regulatory constraints such as South Africa's restriction on drone flights within 10 km of airstrips and during nighttime pose additional challenges. A solution is needed that combines high-resolution imaging with scalability to meet the demands of large PV installations.

2 Theory

Crystalline silicon (c-Si) PV modules typically consist of a glass front cover, a polymeric encapsulant layer, followed by mono- or polycrystalline silicon cells, another polymeric encapsulant layer, and a polymeric back sheet or glass in the case of a bifacial PV module [6]. A standard photovoltaic (PV) module production process typically includes the following steps: glass washing and drying; tabbing of cell ribbons and soldering of the cell matrix; module lay-up with cross-connection soldering; embedding of the module layers; edge sealing and framing; junction box attachment; and final power measurement [6]. Embedding in terms of PV modules is the process in which the cell matrix is placed into a PV module. There a several types of embedding, but all experience challenges to achieve uniform and sufficient curing or cross-linking levels to ensure strong adhesion and stable laminates.

The decrease in efficiency and lifespan of a module is attributed mostly to optical degradation and electrical mismatch [7]. Optical faults are the result of poor quality of the encapsulant layer, prolonged exposure to high temperatures and humidity, and ingress of oxygen into the module, accelerating corrosion [7], [8]. Figure 1 shows the process of water or oxygen ingress into the PV module through the backsheet and into the encapsulant layer, resulting in a change in the composition of the encapsulant known as quenching [8]. This change in composition of the encapsulant has an effect on the fluorescence of the material and thus will fluoresce at a different wavelength, allowing for identification of microcracks in a PV cell that are not seen with visual imaging [8]. This highlights the need for multiple image techniques to fully understand the performance of a PV module.

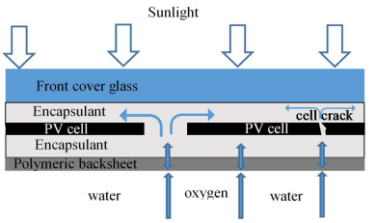

Figure 1. Ingress of water and oxygen into a PV module [8]

Multiple types of imaging techniques are used to fully characterise a PV module. For example, detection techniques employed to identify optical failures are different from those employed for the detection of electrical failures. Optical failures may be seen by the naked eye, such as visual imaging or UVF, whereas electrical losses resulting from defects such as cracked cells or a disconnected string require electroluminescence imaging [4]. Visual imaging can be performed by the naked eye at an illumination level of 1000 lux and requires basic imagery equipment [4]. Due to this effect, EL imaging is one of the most common imaging techniques used.

Traditional methods of imaging are comprised of two fields, laboratory- and field-based [9]. Laboratory-based testing is optimum for testing such as EL, as lighting and external interference can be minimised [9]. However, with the development of large-scale PV plants a field-based testing is needed [9]. Field testing relies on labour extensively, requiring additional time and resources, leading to a limit to the number of modules that can be tested within a reasonable amount of time [9]. A team at Sandia National Laboratories proposed a solution to this problem by developing a robot PV monitoring system that reduced human intervention, allowing for adaptably to different-sized PV systems and imaging techniques [10]. This work is similar in that automated image capture and basic processing as an expected outcome that has a direct application in the PV industry.

3 Methodology

To develop an on-site imaging system, a lab-based prototype was first required to test the camera hardware, control systems, and image processing software. The implementation of this prototype, referred to as the "Gantry," followed a structured process. First, the problem was defined, and a design solution proposed. Next, both electrical and mechanical components were modelled in SolidWorks. The Gantry was then constructed based on the CAD model, and a software control system was developed. Finally, a Python script was implemented to stitch the captured images into a single high-definition composite.

3.1 Definition of Problem and Proposed Solution.

The problem definition established the need to capture high-definition images using various imaging techniques to identify faults within PV modules. The system must be semi-autonomous, requiring only relative information about the module and the selected imaging technique. It should feature a user interface for operator interaction and store captured images for later access. Additionally, the system must support multiple cameras and accommodate additional sensors for testing purposes. It should be adaptable to different module sizes and designed to serve as the foundation for a fully on-site imaging system.

A proposed solution was developed in which the system is controlled by a Raspberry Pi for high-level operations and user interface, while an Arduino Mega handles low-level control tasks. The mechanical design follows a two-axis, dual-drive configuration utilizing three stepper motors to ensure precise movement. The system accommodates PV modules up to 2.4 × 1.3 meters, covering the size range of most modern modules. A Python script facilitates communication between the Raspberry Pi, camera, sensors, microcontroller, and operator, providing comprehensive system control and support for all integrated features.

3.2 Design and Construction of the Gantry.

The CAD model of the gantry is shown in Figure 2. The structure of the gantry is built from 45 x 45 mm Bosch Rexroth extrusion to allow for the ease of assembly and any modification needed. The design uses a dual-drive motor setup whereby the Y axis is controlled by two NEMA 32 stepper motors to reduce racking caused by the large design. The X axis is controlled by another NEMA 32 motor mounted to the axis or 'rack'. Additionally, the rack is built from a 20 x 40 mm V slot extrusion with a V-Plate as the end effector, which allows for the mounting of a Raspberry Pi 5 8gb with a Pi-Camera 3 NOIR 12MP and a Sony IMX477 12 MP camera. Each axis is driven with V belt and pulley with a minimum resolution of 0.1 mm/step on the X axis and 0.18 mm /step on the Y axis.

The design incorporates 3D printed components for rapid prototyping of custom parts, as shown in the figure 3, where a bracket securely holds the Raspberry Pi, cameras, and additional sensors mounted to the V-Plate. The Raspberry Pi manages the high-level system control and provides a user interface via a Python script. It communicates with an Arduino Mega 2560 microcontroller over USB using serial communication to manage low-level tasks such as controlling the stepper motors, reading sensor inputs, handling user interfaces, and monitoring an emergency stop button. The Arduino, along with the motor drivers, power supplies, and physical interface components, is housed in a ventilated control box, shown in Figure 4. Manual control of the system can be performed using onboard buttons and a joystick, without requiring communication with the Raspberry Pi.

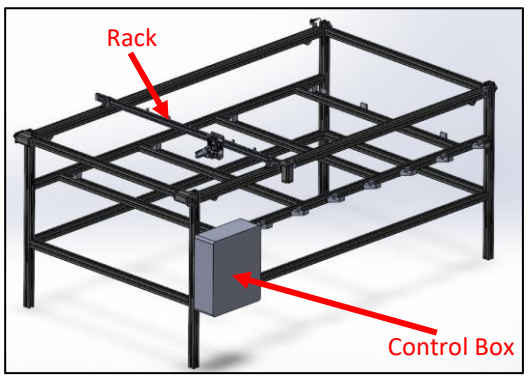

Figure 2. CAD design of Gantry

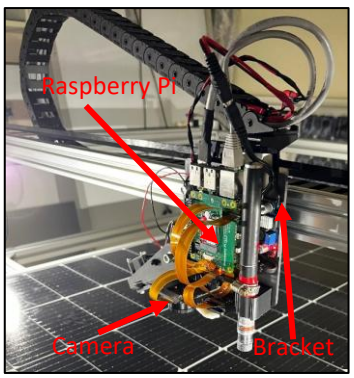

Figure 3. Raspberry Pi and Sensors

Figure 4. Control Box

3.3 Image capture, stitching, and processing.

The image capture sequence begins by entering the setup through a Python command prompt. During setup, the user inputs the dimensions of the PV module, selects the desired camera, and chooses between UV or visual imaging. Once configured, a 3D array of positional coordinates is generated to define all target locations. The Raspberry Pi then sequentially sends each position to the Arduino. When the Arduino confirms it has reached the specified position, the Pi captures an image using the selected camera. Each captured image is stored on a 500GB SSD HAT and tagged with an identifying position for traceability. The ID tag in each photo is identified as CXRYCZ where X refers to the position in the X-axis range starting from 0, and right to left of the module when viewed from the front in portrait orientation. Y is similar to X but defines the row number from top to bottom of the PV module. The determination of positions of positions in the array of coordinates is determined by the camera selected, the size of the module, and the overlap of images for stitching.

4 Results and Discussion

Two fault detection techniques were used, viz. visual imaging and ultra-violet fluorescence (UVF) imaging. To increase the lighting and reduce glare from laboratory lighting, four 10 W cool white (6000 K) lights were used to illuminate the module. Each module was cleaned thoroughly before testing, as the main scope was to detect permanent damage/faults within the module.

4.1 Challenges with image capture and stitching.

Capturing and stitching images to create a cohesive, single image is a complex task that requires both advanced computational processing and precise mechanical design. One of the challenges encountered is image overexposure caused by reflections from the extrusion frame under LED illumination. This issue can be mitigated by applying a non-reflective film over the extrusion frame to reduce glare. Another challenge includes stitching difficulties, particularly at the image edges, where alignment may fall within a cell rather than between them. Although machine vision software such as OpenCV, which relies on pattern recognition, has been employed, the repetitive and featureless nature of PV modules limits its effectiveness. As a result, a more reliable approach involves precise mechanical indexing of the module and implementing edge detection to identify full cell boundaries. This ensures stitching is performed at consistent locations outside the edges of each cell, improving alignment and overall image quality.

4.2 Image processing and correction.

To improve the quality of the final stitched image, each image must first be rotated and corrected for distortion before stitching can occur. The rotation process is illustrated in the Figure 5, beginning with the initial image capture (A). A greyscale mask is then applied to enhance edge visibility (B), followed by a binary threshold to reduce noise and isolate key features (C). OpenCV's edge detection is subsequently used to identify points of interest in the image (D). Based on these detected edges, OpenCV generates lines and computes their equations (E), typically identifying either the cell fingers or the cell's outer edge if the fingers are not visible. Lines with angles greater than 5 degrees from horizontal are discarded, and the image is rotated using the median angle of the remaining lines (F). Since rotation introduces void regions along the image edges, the final step is to crop the image to remove these empty borders (G).

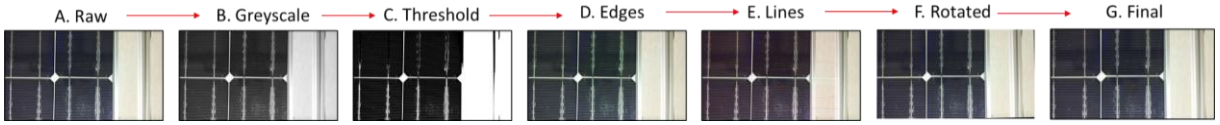

Figure 5. Process of image correction for a single image before stitching

Figure 6 shows a stitched 540 W module with dimensions of 1130 x 2260 mm, this being one of the largest modules able to be tested by the gantry. Images were captured using Raspberry Pi Camera 3 NOIR with 12 MP resolution. Each Image size is roughly 1.9 MB, with a total of 56 images captured, resulting in a 223.6 MB image when stitched together. Basic image stitching and blending are performed after the images are captured.

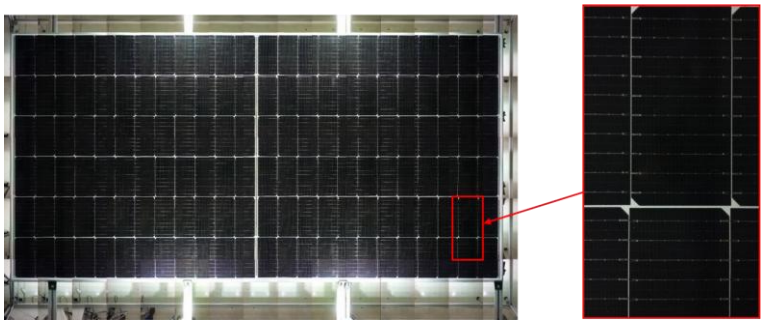

Figure 6. Stitched visual image of large PV module with reference to a single image

4.3 Faults and Defects: Visual Imaging

Several modules were tested using the visual imaging system developed. Figure 7 highlights both manufacturing defects in PV modules and permanent damage caused by prolonged environmental exposure after installation. Manufacturing faults such as trace misalignment, irregular cell patterns, and finger defects can introduce minor mismatches within the module, leading to reduced power output. Edge chips, often caused during the doping process of the silicon cell, can act as stress concentrators and result in cracks due to mechanical impact or thermal cycling. These cracks may propagate, leading to microcracks, cell disconnects, and further degradation of both the module's performance and lifespan. Additional defects shown in the figure include cell delamination and flux oxidation, which reduce module efficiency by generating localized heat and applying thermal stress to affected cells. The scratch seen in Figure 7 is caused by contact with the frame of another module, depositing aluminium onto the glass surface; this scratch is considered non-permanent and does not affect performance significantly.

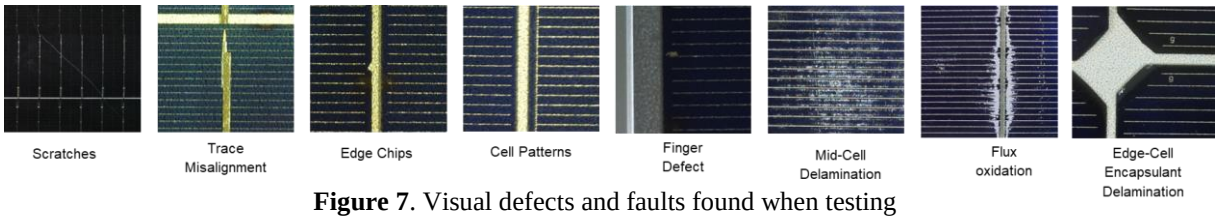

Figure 7. Visual defects and faults found when testing

4.4 Faults and Defects found using UVF Imaging.

Several modules were tested using UVF imaging, and the following results were obtained from the module shown in Figure 8. The figure illustrates a module whose backsheet fluoresces when exposed to ultraviolet light. A low-pass filter (LEE Filter 101 Yellow) was used to reduce glare and saturation in images captured by the Raspberry Pi 3 NOIR camera. Figure 9 reveals evidence of fluorescence quenching, a phenomenon where the module's encapsulant is exposed to moisture or oxygen through the backsheet. This exposure alters the molecular structure of the polymer, thereby changing its fluorescence behaviour under UV light. Additionally, figure 10 shows a localized area within one cell exhibits unexpected fluorescence, which may be due to a small hole in the cell or a deposit of fluorescent material from the backsheet onto the cell's front surface. This hole is also visible in the standard visible spectrum, suggesting a physical defect within the cell. If present, such a defect can lead to cracking of the cell, ultimately decreasing the power output and shortening the lifespan of the module.

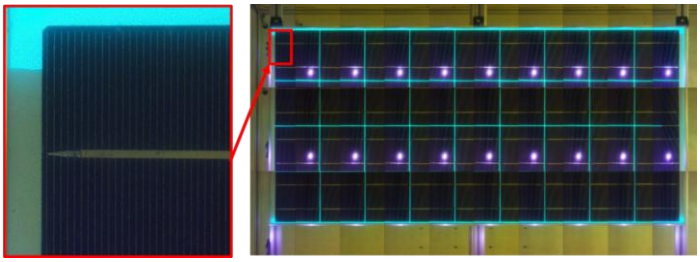

Figure 8. Stitched UVF image with indication of fluorescent material

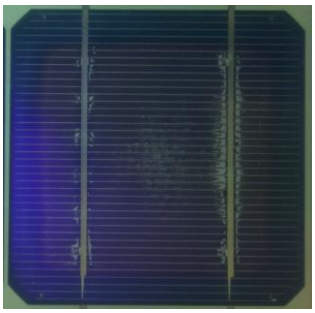

Figure 9. UVF: Quenching pattern

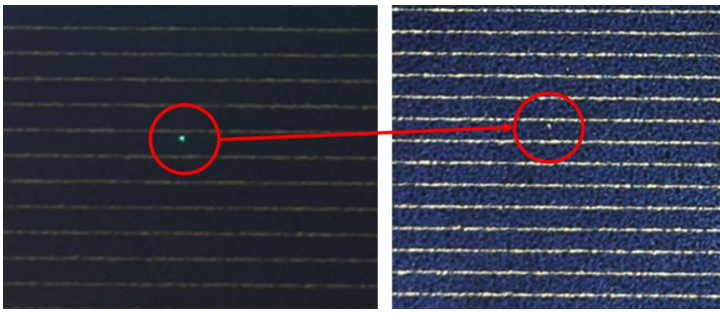

Figure 10. Hole in cell

5 Conclusion

The development and testing of a laboratory-based imaging gantry for automated visual and UVF inspection of PV modules demonstrates a promising approach for high-throughput, high-resolution fault detection. The system integrates precise mechanical motion control, modular hardware, and advanced image processing to provide detailed insights into both manufacturing defects and long-term degradation of PV modules. Key features include a robust mechanical design, adaptable imaging modes, automated image capture, and custom stitching algorithms capable of producing large composite images suitable for diagnostic analysis.

Preliminary results confirm the system's effectiveness in detecting common visual and UVF-related faults, such as edge chipping, cell delamination, and quenching caused by encapsulant degradation. Although challenges remain—particularly in image alignment and illumination conditions—preprocessing techniques such as edge detection, rotation correction, and cropping have led to significant improvements in overall image quality and stitching accuracy. However, further refinement is still required.

This proof-of-concept system establishes a solid foundation for future on-site deployment, where the methodology can be scaled to accommodate utility-scale PV installations. Future work will focus on enhancing image processing and stitching algorithms, incorporating additional testing techniques such as electroluminescence (EL), and increasing automation to enable real-time, large-scale PV inspection with minimal human intervention.

6 Acknowledgements

The authors wish to acknowledge assistance from colleagues and financial support from Nelson Mandela University and the Department of Science Technology and Innovation of South Africa.

7 References

[1] Wu, J. Zhu, T. R. Betts, and R. Gottschalg 2014 *Prog. Photovolt.: Res. Appl*. **22** 796–809
[2] S. R. Madeti and S. N. Singh, 2017, Sol. Engy. , **158**, 161–185
[3] I. Polymeropoulos, S. Bezyrgiannidis, E. Vrochidou, and G. A. Papakostas, 2024, MDPI Tech., **12**
[4] H. Al Mahdi, P. G. Leahy, M. Alghoul, and A. P. Morrison, 2024, MDPI Tech. **4** 43–82
[5] V. Carletti, A. Greco, A. Saggese, and M. Vento, 2020, J Amb. Int. Hum. Comp. **11** 2027–40
[6] C. W. Hilti, I. Haedrich, and K.-A. Weiss, 2013, Photo. Int. 85–92
[7] D. Wu, J. Zhu, T. R. Betts, and R. Gottschalg, Prog. Photovolt.: Res. Appl. **22** 796–809
[8] F. Vorster and E. Van Dyk, Proceedings of the 6th Southern African Solar Energy Conference (SASEC), 2019, East London, ISBN 978-0-7972-1825-3
[9] R. del Prado Santamaría, M. Dhimish, G. A. dos Reis Benatto, T. Kari, P. B. Poulsen, and S. V. Spataru, MDPI Tech., 2025, **16**
[10] M. Y. Vazquez Nieves, A. M. Colón González, and J. L. Braid, 2023, Inst. of Ele. and Electr. Eng. Inc.